Electronic Supplementary Material (ESI) for Nanoscale.

Quantum Capacitance-Limited MoS_2 Biosensors Enable Remote Label-Free Enzyme Measurements

Son T. Le[1,2], Nicholas B. Guros[3,4], Robert C. Bruce[1], Antonio Cardone[5,6], Niranjana D. Amin[7], Siyuan Zhang[1,2], Jeffery B. Klauda[4], Harish C. Pant[7], Curt A. Richter[1] and Arvind Balijepalli[3,*]

[1]Nanoscale Device Characterization Division, National Institute of Standards and Technology, Gaithersburg, MD 20899, USA ; [2]Theiss Research, La Jolla, CA 92037; [3]Microsystems and Nanotechnology Division, National Institute of Standards and Technology, Gaithersburg, MD 20899, USA;[4]Department of Chemical and Biomolecular Engineering, University of Maryland, College Park, MD 20742, USA; [5]Software and Systems Division, National Institute of Standards and Technology, Gaithersburg, MD 20899, USA; [6]University of Maryland Institute for Advanced Computer Studies, University of Maryland, College Park, MD 20742, USA; [7]National Institute of Neurological Disorders and Stroke, National Institutes of Health, Bethesda, MD 20892, USA

*e-mail: arvind.balijepalli@nist.gov

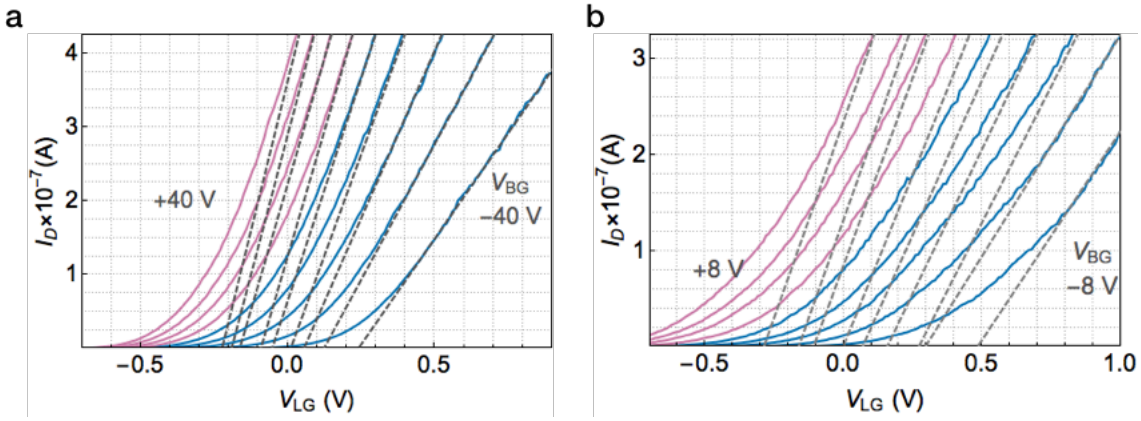

Fig. S1: The coupling between the ionic liquid and back gates was estimated from the transfer characteristics of the device. (*a*) When the back gate oxide thickness, d=300 nm, $\alpha = V_{BG}/V_{t,LG}$ was estimated to be 159 from the back gate voltage, V_{BG}, and shift in the liquid gate threshold voltage, $V_{t,LG}$. (b) When d=70 nm, α was lower as expected and estimated to equal 40.

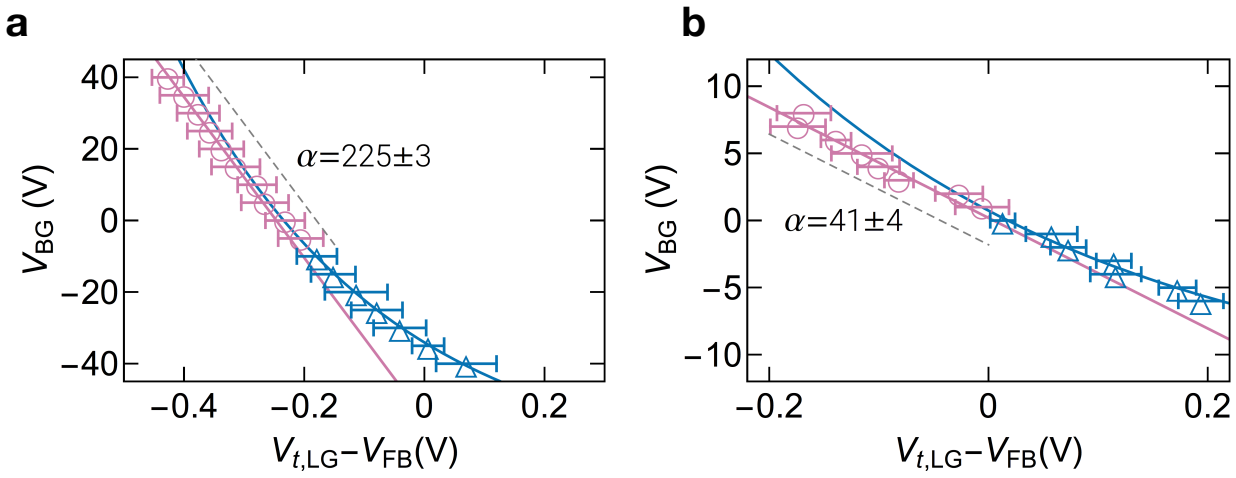

Fig. S2: The shift in the back gate voltage (V_{BG}) plotted against the liquid gate threshold voltage ($V_{t,LG}$) allowed the estimation of the gate coupling ratio (α). The flatband voltage (V_{FB}) in both cases was assumed to be 0. (*a*) When the back gate oxide thickness (*d*) was 300 nm, the maximum value of α was estimated to be 225±3. (b) The corresponding maximum value of α when *d*=70 nm was 41±4.

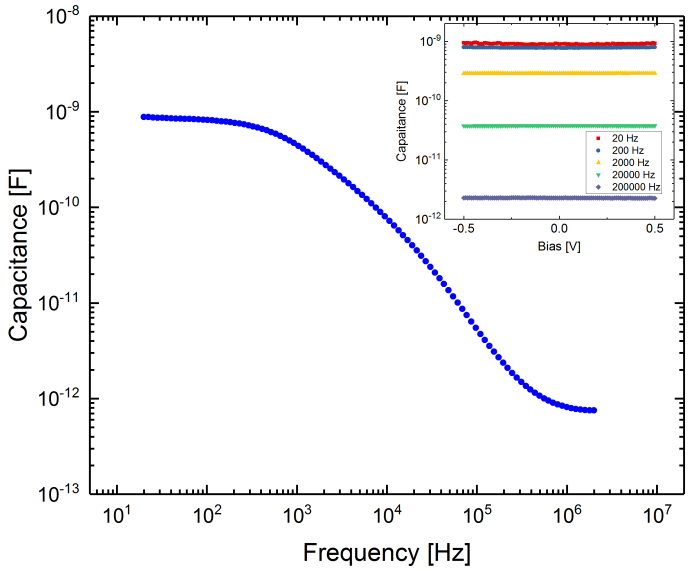

Fig. S3: AC impedance data for ionic liquid on gold electrodes. V_{AC} = 10 mV, bias = 0 V. (inset) Capacitance with fixed frequency and measured with a variable voltage bias. We extracted the quantum capacitance value following a standard practice used previously when analyzing the performance of ionic liquid gated MoS_2 field effect transistor (Refs. 30 and 32 of the main text). Since, the quantum capacitance is an intrinsic property of MoS_2 and it depends on the carrier concentration within the channel, we are not aware of a way to directly measure its value outside of a field-effect-transistor (FET) structure, and in particular without coupling the channel to a gate dielectric to control the carrier density. Here, we performed a separate measurement of the capacitance of the room temperature ionic liquid used as the top gate dielectric. The measured ionic liquid gate capacitance value allowed us to extract the maximum quantum capacitance value of MoS_2 channel using model presented in the Method section. The extracted value compares favorably with both theory and previous experiment data confirming the approach of the method that we used in this paper.

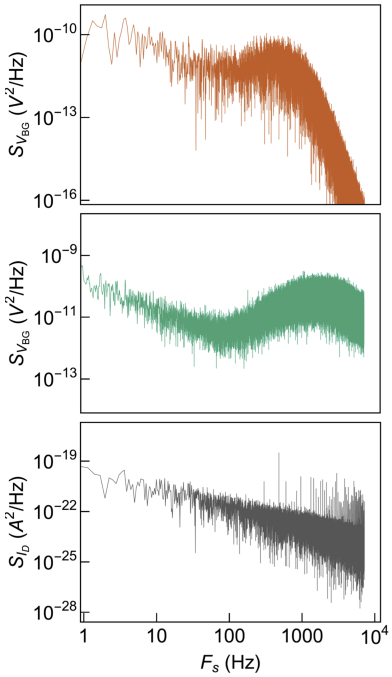

Fig. S4: The power spectral density of V_{BG} (300 nm SiO_2, *top* and 70 nm SiO_2 *middle*) under PID control and I_D (300 nm SiO_2, *bottom*) under open loop operation were used to estimate the signal to noise ratio (SNR).

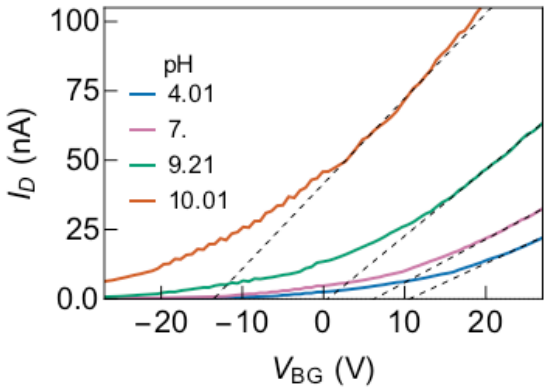

Fig. S5: The response of the sensor to standard pH buffers was estimated from the device transfer curves. The threshold voltage of the back oxide gate decreased when the solution pH measured with the ionic liquid gate became more acidic. The threshold voltage exhibited linear relationship with the solution pH over a wide range.

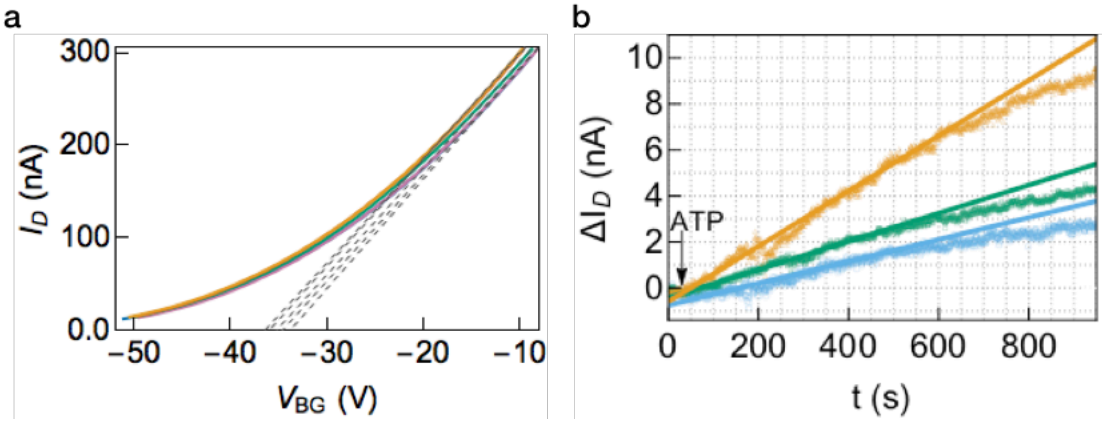

Fig. S6: Changes in the solution pH during enzyme catalyzed phosphorylation were used to estimate Cdk5 activity and dynamics. (a) Steady state measurements of the change in sensor I_d-V_{BG} characteristics allowed the estimation of phosphorylation as a function of the substrate protein concentration. (b) The measurements were also performed dynamically by recording the current across the field effect transistor (FET) channel upon the initiation of the phosphorylation reaction with ATP for three concentrations of the substrate protein.

Detailed Derivation of the Relationship Between the Gate Capacitances and Voltages

The detailed derivation of the relationship between C_{TG}/C_{BG} and $dV_{BG}/dV_{t,LG}$ follows a classical model developed by Lim *et. al*[1] and later adapted by Jang *et. al* [2-4] for the case of ion sensing Si-FET and ionic liquid-gated MoS_2 FET. Fig. S3 depicts a simplified one-dimensional view of the active region of a dual-gated metal-oxide semiconductor field-effect transistor (MOSFET).

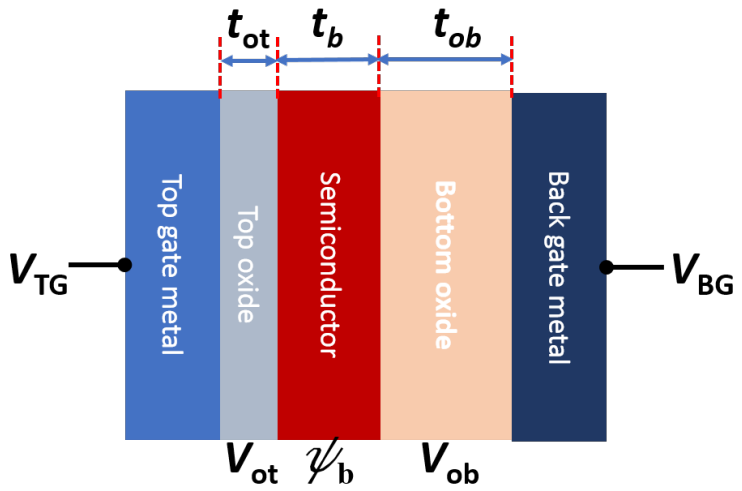

Fig. S7: One-dimensional active portion of the dual-gated field effect transistor (FET). For simplicity, the back gate is labeled "Back gate metal" even though it is typically heavily doped Si.

In analogy to bulk MOSFET theory,[5] we can write:

$$V_{TG} = \psi_{ST} + V_{ot} + F_{t,MS} \quad (1)$$

and

$$V_{BG} = \psi_{SB} + V_{ob} + F_{b,MS} \quad (2)$$

where V_{TG} and V_{BG} are the top and back gate voltages, ψ_{ST} and ψ_{SB} are the top and back surface potential at the semiconductor top and bottom oxide interfaces respectively, V_{ot} and V_{ob} are the potential drop across the top and back gate oxide, $F_{t,MS}$ and $F_{b,MS}$ are the differences in the metal and semiconductor work-functions.

Under normal operating conditions, the semiconductor is completely depleted. The potential drop across the semiconductor is then given by the expression:

$$\psi_b = \psi_{ST} - \psi_{SB} = (E_{st} - qt_bN_a/(2e_s))*t_b \quad (3)$$

where ψ_b is the potential drop across the semiconductor, E_{st} is the electric field at the top-surface edge of the depletion region, and N_a is the doping density of the semiconductor (assuming p-type for an n-channel MOSFET), t_b is the thickness of the semiconductor, and ε_s is the semiconductor dielectric constant.

Using Gauss's theorem for the top oxide semiconductor interface

$$V_{ot} = 1/C_{ot}*(\varepsilon_s E_{st} - Q_{ct}) \quad (4)$$

Similarly, for the bottom oxide semiconductor interface

$$-V_{ob} = 1/C_{ob}*(\varepsilon_s E_{st} - qN_a t_b - Q_{cb}) \quad (5)$$

where $C_{ot(b)}$ is the top(bottom) oxide capacitance, $Q_{ct(b)}$ is the inversion charge at the top(bottom) oxide/semiconductor interface. For simplicity, we did not take into account the fix charges and the interface states at the interfaces. Using equations 1, 3, and 4 we obtain:

$$V_{TG} = (1+ C_b/C_{ot})\psi_{ST} - C_b/C_{ot}*\psi_{SB} - (Q_b/2+ Q_{ct})/C_{ot} + F_{t,MS} \quad (6)$$

where $C_b = \varepsilon_s/t_b$ is the depletion charge capacitance and $Q_b = - qN_a t_b$ is the depletion charge density. Similarly using equations 2, 3, and 5 we obtain:

$$V_{BG} = (1+ C_b/C_{ob})\psi_{SB} - C_b/C_{ob}*\psi_{ST} - (Q_b/2+ Q_{cb})/C_{ob} + F_{b,MS} \quad (7)$$

Equation 6 and 7 describe the coupling between the front and back gate potentials. When the back oxide/semiconductor interface is in the inversion or accumulation regime, the top gate threshold voltage is virtually independent of the back gate voltage.[1]

On the other hand, when considering the case of depleted back oxide/semiconductor interface, the threshold condition of the top oxide/semiconductor interface is $\psi_{ST} = 2F_B$ where $F_B = (kT/q)*\ln(N_a/n_i)$ where k is Boltzmann constant, T is temperature and n_i is the semiconductor intrinsic carrier density.

Using equations 6 and 7, the top gate threshold voltage depends on back gate voltage using the relationship:

$$V_{t,TG} = V_{t,TG,A} - C_b C_{ob}/(C_{ot}(C_b+C_{ob}))*(V_{BG} - V_{BG,A}) \quad (8)$$

where the constants $V_{t,TG,A} = (1+ C_b/C_{ot})\, 2F_B - Q_b/2C_{ot} + F_{t,MS}$ and $V_{BG,A} = F_{b,MS} - C_b/C_{ob}*2F_B - Q_b/2C_{ob}$.

From equation 8, we have:

$$\boldsymbol{\Delta V_{t,TG} = -\, C_b C_{ob} / (C_{ot}(C_b + C_{ob})) * \Delta V_{BG}} \quad \textbf{(9)}$$

In order to apply equation 9 to our ionic-liquid gated MoS_2 FET, we need to modify the model slightly. For a monolayer MoS_2, t_b is ~ 0.7nm, which in turn causes $C_b >> C_{ob}$. Additionally, $C_{ob} \approx C_{BG}$ and C_{ot} need to be replaced by $C_{LG} = C_{ot}\, C_Q/(C_{ot} + C_Q)$ to take into account the effect of the quantum capacitance. Finally, equation 9 must be rewritten as:

$$\boldsymbol{\Delta V_{t,TG} = -\, C_{BG}/C_{LG} * \Delta V_{BG}} \text{ or } \boldsymbol{\Delta V_{BG} = -\, C_{LG}/C_{BG} * \Delta V_{t,TG}} \quad \textbf{(10)}$$

The negative sign in equation 10 implies that increasing V_{BG} will decrease $V_{t,TG}$ since it is easier to accumulate carriers in the channel at positive back gate voltages.

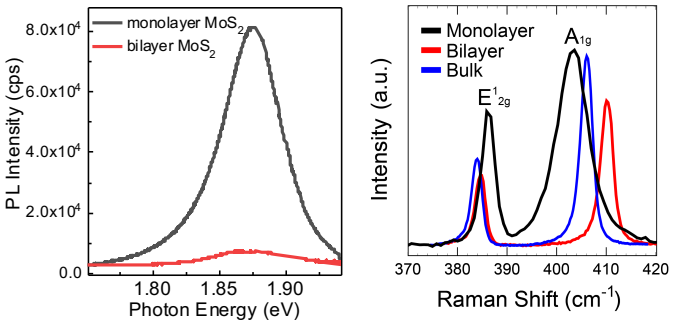

Fig. S8: (*left*) Photoluminescence (PL) spectra of monolayer and bilayer MoS_2. Monolayer MoS_2 (*black*), which was used to fabricate devices in this study, possess a direct bandgap and exhibit a high PL intensity and a peak at ≈1.87 eV. In contrast, bilayer MoS_2 (*red*), which has an indirect bandgap has a greatly reduced PL intensity. (*right*) Raman spectra of MoS_2 used in this study. The A_{1g} and E_{2g} peak frequencies of 404.1 cm^{-1} and 385.0 cm^{-1} were used to verify that the film was a monolayer (*black*). The peak shifts of bilayer (*red*) and bulk films (*blue*) exhibit a distinct shift in the Raman peaks. *Adapted with permission from Guros et. al.*[6] *Copyright 2019 American Chemical Society.*

References:

1 H. K. Lim and J. G. Fossum, *Electron Devices, IEEE Transactions on*, 1983, **30**, 1244–1251.
2 H.-J. Jang and W.-J. Cho, *Sci Rep*, 2014, **4**, 5284.
3 M. M. Perera, M.-W. Lin, H.-J. Chuang, B. P. Chamlagain, C. Wang, X. Tan, M. M.-C. Cheng, D. Tománek and Z. Zhou, *ACS Nano*, 2013, **7**, 4449–4458.
4 L. Chu, H. Schmidt, J. Pu, S. Wang, B. Özyilmaz, T. Takenobu and G. Eda, *Sci Rep*, 2014, **4**, 7293.
5 S. M. Sze, *Physics of Semiconductor Devices*, Wiley-Interscience, 1981.
6 N. B. Guros, S. T. Le, S. Zhang, B. A. Sperling, J. B. Klauda, C. A. Richter and A. Balijepalli, *ACS Appl. Mater. Interfaces*, 2019, **11**, 16683–16692.